

Spectral Evolution of Hercules X-1 over Main High State from RXTE/PCA Observations

Denis A. Leahy^{1*}, Mohammed H. Abdallah²

¹Department of Physics and Astronomy, University of Calgary, Calgary, Canada

²Astronomy Department, National Research Institute of Astronomy and Geophysics (NRIAG), Cairo, Egypt

Email: *ms_ali80@yahoo.com

How to cite this paper: Leahy, D.A. and Abdallah, M.H. (2022) Spectral Evolution of Hercules X-1 over Main High State from RXTE/PCA Observations. *Journal of High Energy Physics, Gravitation and Cosmology*, 8, 896-918.
<https://doi.org/10.4236/jhepgc.2022.84061>

Received: June 27, 2022

Accepted: August 28, 2022

Published: August 31, 2022

Copyright © 2022 by author(s) and Scientific Research Publishing Inc. This work is licensed under the Creative Commons Attribution International License (CC BY 4.0).

<http://creativecommons.org/licenses/by/4.0/>



Open Access

Abstract

We test different X-ray spectrum models to find the one that best represents the observed Rossi X-ray Timing Explorer/Proportional Counter Array (RXTE/PCA) spectra of Her X-1 during Main High state (MH). We then apply this model to MH observations taken over the lifetime of RXTE. From the results, we obtain patterns in the spectral parameters vs. 35-day phase during MH. The precessing-disc occultation model explains the 35-day cycle by changes in observer view of the emission regions by the accretion disc 35-day precession. Qualitatively, we find that this model can describe the main spectral changes. However, several spectral parameters show detailed changes that the models have not addressed yet. These changes will likely require modifications to the basic precessing-disc model for the 35-day cycle.

Keywords

X-Ray Binaries, Hercules X-1, X-Ray Spectrum

1. Introduction

Hercules X-1 (Her X-1) is a well-studied X-ray binary with 1.7-day orbital period and 35-day long-term period [1] [2]. The 35-day period is caused by the precessing accretion disc around the neutron star, which causes periodic obscuration of the X-ray emitting accretion column on the neutron star [3]. The 35-day cycle normally shows a few day variations in its period [2] [4], but sometimes disappears for a few to several months: these periods are called anomalous low states (ALS) [5].

There are different physical origins for the X-ray emission from the system Her X-1/HZ Her. The X-ray emission regions consist of the following components: 1) Direct X-ray beams (pencil and/or fan beam) originating in the accre-

tion column of the accreting pulsar Her X-1 [6]; 2) Weak isotropic emission high above the accretion column resulting from Thomson scattering of the direct X-rays [3]; 3) Soft emission below keV, modelled by a black-body of temperature $kT = 0.1$ keV, resulting from reprocessing of the hard X-rays in the outer neutron star magnetosphere and/or the inner edge of the accretion disc [7]; 4) Reflection of the direct X-ray emission by the illuminated inner edge of the disc [8] and the irradiated face of the companion star [9]; 5) Very weak (at 1% of the direct flux) un-pulsed scattered emission by an extended accretion disc corona which is present throughout the 35-day cycle [10].

These emission regions are periodically covered/uncovered by the accretion disc every 35-days. At the turn-on of both high states, the outer edge of the disc clears the line of sight to the central source, while the gradual flux decay near the end of both MH-state and SH-state is due to a gradual covering of the emission regions by the near side of the disc inner edge [8]. In the low state, the central emission regions are continuously covered by the intermediate rings of the disc.

Reference [8] constructed a set of models of increasing complexity (numbered model-1 to model-7) for the accretion disc and the central source to fit the ASM light curve of the 35-day cycle. These models considered pulse-phase-averaged emission, thus the central source is considered as a steady point source and/or a steady extended emission region. This central source is periodically occulted by the inner edge, outer edge, and intermediate rings in the disc as the disc rotates over 35 days.

The best fit model that gives a good fit to the pulse-phase-averaged ASM light curve and is consistent with the pulse-evolution model of [3] is model-7. Model-7 consists of: 1) a slightly extended central source with a total intensity of 12.9 ± 2.9 counts/s in ASM, that is partially seen with different degrees during MH-state and SH-state; 2) reprocessed radiation by the far side of the inner edge of the disc with intensity 2.1 ± 0.7 counts/s in ASM; 3) a two-layer atmosphere at the outer disc edge (cold-thin atmosphere and hot-thick atmosphere with scale-heights of 6.9×10^8 cm and 4.7×10^{10} cm (respectively).

The outer disc radius is $R_o = 2 \times 10^{11}$ cm, the inner disc radius is $R_i = 4 \times 10^7$ cm and the central source emission region is of size $R_c = 2.7 \times 10^6$ cm. Thus the central source is seen as a point source by the outer disc edge, while of significant angular size as viewed by the inner disc edge. The sharp turn-on of the MH-state is due to the uncovering of the central source from behind the cold-thin atmosphere in the outer disc-edge. Following the sharp turn-on, a gradual increase in flux occurs when the hot-thick atmosphere gradually clears our line of sight to the central source. A similar sequence of events occurs during the SH-state turn-on. This is illustrated in Figure 5 and Figure 6 of [8]. The central emission is occulted by the near side of the inner disc edge during the decay of both high states. Thus the source geometry is a key to the time dependence of the decay of high states. The near side of the inner disc edge partially covers the central source during the early MH-state and SH-state to different degrees.

Another source of emission comes from the reprocessed/reflected radiation

off of the illuminated far side of a thick inner disc edge. The inner ring is tilted and precessing over the 35-day cycle, so the central source is most clearly viewed twice per 35-day cycle: when the ring axis is pointing most toward us at the peak of the MH-state; and when the ring axis is pointing most away from us, at the peak of SH-state. Also as can be seen from Figure 9 of [8], the far inner edge of the disc will be gradually occulted by the near inner edge of the disc. Using these two emission regions (*i.e.* central source and reflected emission by the inner ring) and the occultation by the disc, [8] reproduced the contribution of both emission regions over the 35-day cycle.

In this work, we make an observational study of the spectral evolution of Hercules X-1 over the Main High state using archival data from the Rossi X-ray Timing Explorer/Proportional Counter Array (RXTE/PCA). In Section 2, we describe the observations and how we choose and test the spectrum model. In Section 3, we give the results of applying the spectrum model to the data. The main results are the spectrum parameter changes as a function of 35-day phase during MH. In Section 4, we discuss these results. The summary is given in Section 5.

2. Observations and Spectrum Analysis

2.1. Observations and Light-Curves

The NASA satellite Rossi X-ray Timing Explorer (RXTE) [11] was designed to facilitate the study of time variability of X-ray sources with moderate spectral resolution. We make use of the data collected by the Proportional Counter Array (PCA) on-board the RXTE. The PCA [12] [13] consists of five identical multi-anode large-area Proportional Counter Units (PCUs).

Her X-1/HZ Her was observed numerous times by RXTE between 1996 and 2005 and the data has been archived at High Energy Astrophysics Science Archive Research Center (HEASARC). The RXTE/PCA database on HZ Her/Her X-1 contains 1.6 Ms of observations. The data were acquired by the RXTE/PCA instrument in the period from February, 1996 to August, 2005 (MJD 50,114 to 53,584) as a result of 23 study proposals for observing the HZ Her/Her X-1 system.

We carried out spectral analysis of PCA standard-2 data of Her X-1 for studying the spectral evolution over the 35-day super-orbital cycle. Standard-2 mode has temporal resolution of 16 s and energy ranges 2 - 60 keV in 129 channels. The times were converted to Dynamical Barycentric Modified Julian Day Time (MJD TDB) using the HEASARC time conversion procedures.

Binary orbital phase was determined using the ephemeris of [14]. To find the 35-day phase we used the nearest last MJD turn-on time of the 35-day cycles and cycles lengths of [15]. To study the spectral evolution over normal 35-day cycles, we removed data that were taken when the system (Her X-1) was in anomalous low state periods. In our data there are two anomalous low state (MJD 51226.4 to 51756.9 and MJD 52950.6 to 53159.4).

Our purpose is studying spectral evolution over the 35-day cycle other than

dips and eclipse, thus we removed all data that falls within the dips and eclipsing periods. Significant changes in the spectra occur during dips [16] (and references therein) and during eclipse periods [17]. These periods include times during which the accretion stream impacts the disc and cover our line of sight to the central source appearing as absorption dips in the light curve [16] resulting in variations of the spectra. Dips times were taken from [16]. Eclipsing periods were filtered out by removing data with orbital phases less than 0.07 or greater than 0.93. After removal, to make sure that no residual dips remain in our data, we calculated the Softness Ratio (SR) defined as band 1 countrate divided by band 3 countrate, where band 1 and band 3 are the count rates in the energy ranges 2 - 4 keV and 9 - 20 keV respectively. We then rejected data points during MH-state and SH-state with $SR < 0.35$. For low states, SR is normally below 0.35, so this rejection was not done for low states. This resulted in a total ALS-eclipse-dips-free exposure of 432 ks. The observations cover parts of twenty different main high states.

The band b and band d light-curves were scaled by the number of active PCUs at any given time to yield count rate per PCU. These and SR are plotted vs. 35-day phase for the Her X-1 data in **Figure 1**.

We observe that the softness ratio is very different during the main high and short high states compared to the low states. As noted previously by [18], the low state data appear similar to the data in main high and short high states when Her X-1 is in a dip. The band 1 and band 3 light-curves, and the band-1/band-3 softness ratio are shown for the individual MH states in **Figures 2-4**. The

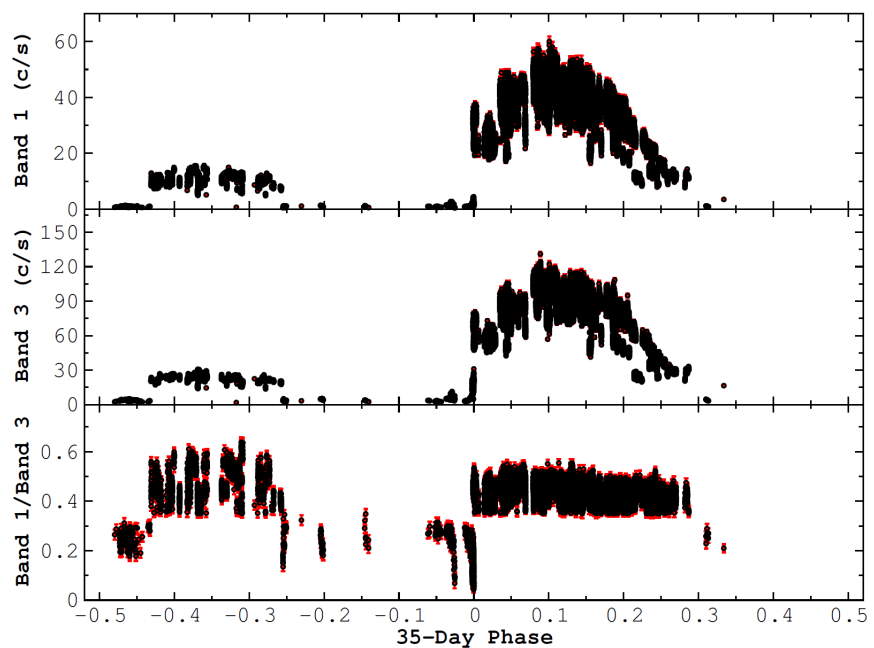


Figure 1. RXTE/PCA count rates for Hercules X-1 as a function of 35-day phase. The band 1 (2 - 4 keV), band 3 (9 - 20 keV) light curves, and the band 1/band 3 softness ratio are shown. The data consist of all standard-2 mode RXTE observations of Her X-1 except for anomalous low states, dips and eclipses.

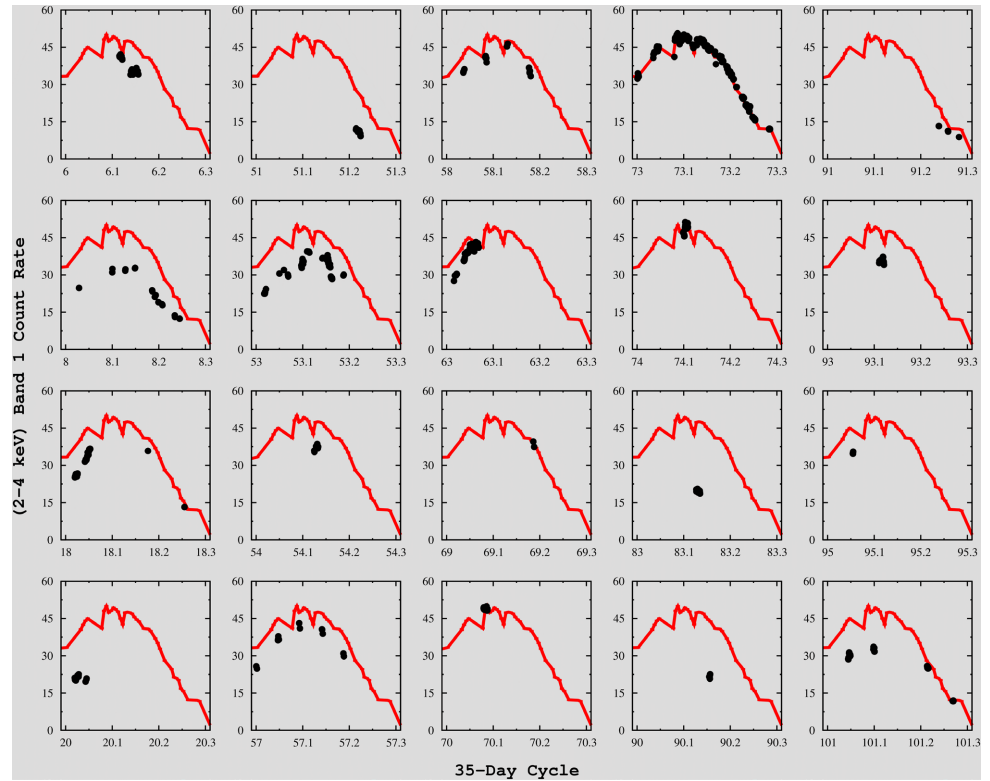


Figure 2. RXTE/PCA band 1 count rates vs 35 day phase for the twenty different main high states observed by RXTE.

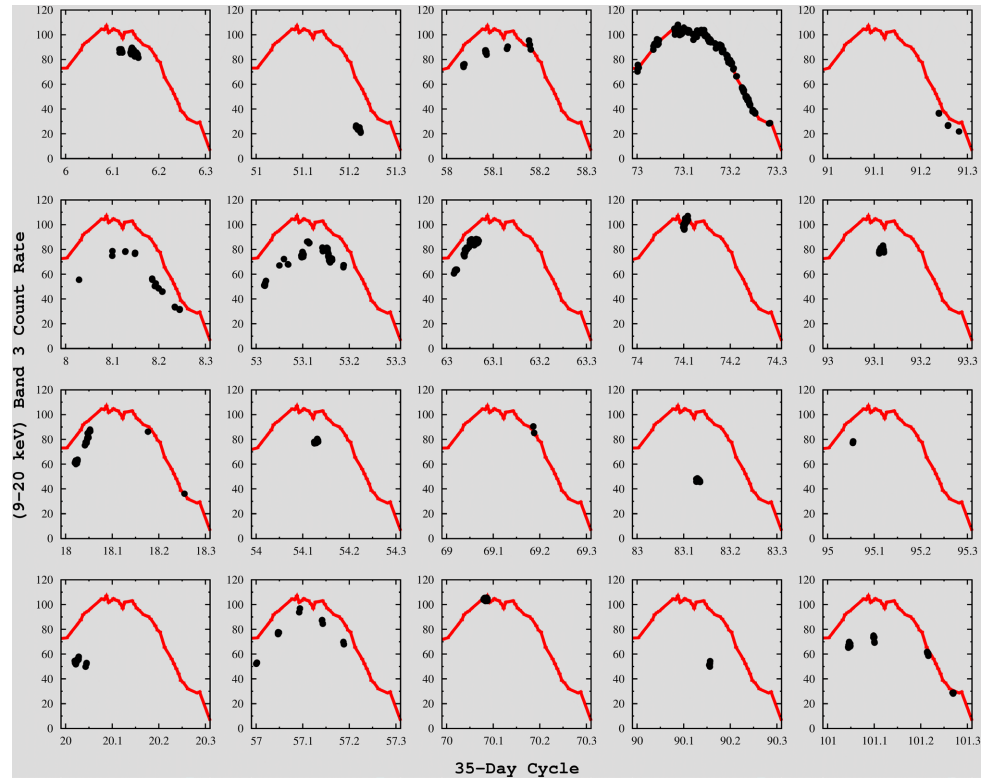


Figure 3. RXTE/PCA band 3 count rates vs 35 day phase for the twenty different main high states observed by RXTE.

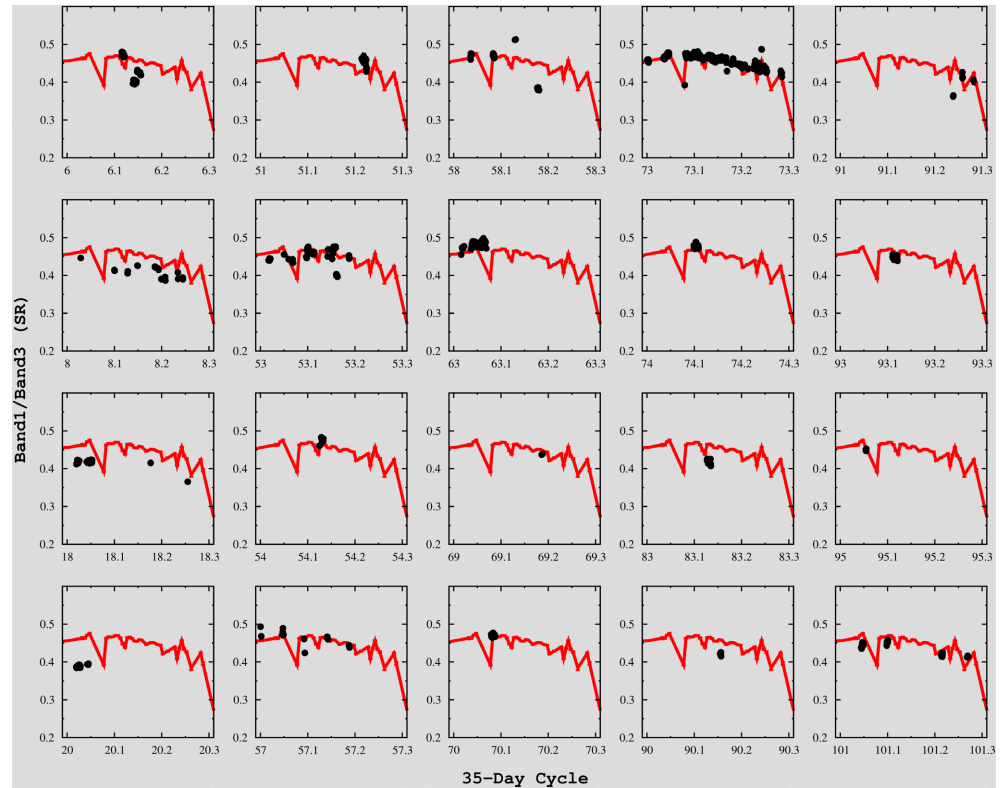


Figure 4. RXTE/PCA band 1/ band 3 softness ratio vs 35 day phase for the twenty different main high states observed by RXTE.

horizontal axis is labelled by 35-day phase, including integer specifying the cycle number. The uneven coverage of different 35-day cycles is apparent. Cycle 73 has the most complete coverage; cycles 8, 18, 53, 57, 58, 63 and 101 have intermediate coverage; and the remaining cycles have very sparse coverage.

The red lines in **Figures 2-4** are linear interpolations through all of the data for cycle 73. They are plotted so that the other cycles can be compared to cycle 73. It is seen from the band 1 and band 3 count rates that most cycles (6, 8, 18, 20, 51, 53, 54, 57, 83, 90, 93, 95 and 101) are fainter on average than cycle 73. The remaining cycles (58, 63, 69, 70, 74 and 91) are nearly the same brightness as cycle 73. From **Figure 4**, the softness ratio vs. 35-day phase is not significantly different for different cycles, except for cycles 8, 18 and 20 (and possibly 83 and 90). These cycles are all fainter than cycle 73 and have lower SR, indicating higher absorption.

2.2. Spectrum Data Processing

In the current work, we make use of the standard-2 PCA data which has a time resolution of 16-s and 129 energy channels that cover the entire energy range (2 - 60 keV) of the PCA detector. We added the data from all three layers and columns of the available PCUs and response matrices were generated accordingly. For Her X-1 we used the faint background model throughout. To obtain better statistics we average over time, to obtain the same signal-to-noise ratio for all of

the spectra. The data were averaged over time intervals between 400-s and 1360-s, with a mean value of 889-s.

We use the graphical user interface (GUI) tool “XDF” (XTE Data Finder) to create a catalogue of files for further analysis. The standard-2 catalogue and the filter file that contains housekeeping parameters and the most recent background model are used to model the background for the selected data using the FTOOLS task “runpcabackest”. We used the FTOOLS task “maketime” to create a good time interval (“.gti”) file selected from the filter file. The criteria chosen for data screening are: 1) The elevation above the Earth must be greater than 10 degrees; 2) The pointing must be stable with 0.02 degrees as an upper limit of the “offset”; 3) All data collected during the passage of RXTE through the South Atlantic Anomaly (SAA) were discarded; and 4) We rejected all data that has “electronX” (X represents the PCU number, 0-to-4) larger than 0.1. The “.gti” file contains the time intervals satisfying the above criteria. The desired spectra are extracted from the standard-2 and background catalogue files in turn, using the FTOOLS task “saextrct”. As we carried out spectral analysis on a large collection of data, a Perl script was written to execute “saextrct” task for all data.

2.3. Spectrum Model Testing

For the purpose of testing different spectral models, energy spectra were extracted with a fixed exposure times of 256 s. For the spectral analysis we used XSPEC. The first three energy channels (<2.5 keV) were ignored because of uncertain background modelling, while channels 59 - 129 (>30 keV) were ignored because of poor counting statistics.

In the 2.5 - 30 keV energy range there are three spectral models commonly used: 1) a power-law times exponential cutoff model [19]; 2) Fermi-Dirac cutoff (FDCO) model [20]; and 3) Negative-Positive EXponential cutoff (NPEX) model [21]. Reference [22] examined the fits with these models, on data obtained for 10 accreting pulsars by PCA/HEXTE instruments on-board of RXTE. They found that the spectral parameters, in both FDCO and NPEX models, show a high degree of correlations. This correlation between spectral parameters makes the search for a best fit difficult and results in larger uncertainties in the obtained values for the parameters. The power-law times exponential cutoff model did not show such high correlations between spectral parameters. Thus following [22], we use the power-law times exponential cutoff model (powerlaw and highecut in XSPEC) for fitting the spectra. In functional form, the model is given as:

$$F(E) = AE^\alpha \quad \text{if } E < E_{cut} \quad (1)$$

$$F(E) = AE^\alpha e^{-(E-E_{cut})/E_{fold}} \quad \text{if } E > E_{cut} \quad (2)$$

where F is the photon number flux, E is the energy, α is the photon index, E_{cut} is the cutoff energy, and E_{fold} is the folding energy.

The discontinuity at the cutoff energy in this model was smoothed by multiplying it by a Gaussian-shaped absorption function (gabs in XSPEC) at the cutoff

energy with width σ_g and depth τ_g fixed at 1.5 keV and 0.35, respectively. The gabs function in XSPEC is given by the equation:

$$\text{gabs} = e^{-\left(\frac{\tau_g}{\sqrt{2\pi}\sigma_g}\right) e^{-0.5((E-E_{\text{cut}})/\sigma_g)^2}} \quad (3)$$

A Gaussian line in emission for the Fe K_α line was also added to the continuum model for fitting the spectra.

This model can be applied to the spectra in three ways: 1) without low energy absorption—we call this the NA model (No-Absorption model); 2) with low energy absorption, called the TA model (Total-Absorption model); 3) partial covering absorption, in which the continuum consists of an unabsorbed continuum component plus an absorbed component, referred to it as PC model (Partial-Covering-model). We have tried all three alternatives in fitting the spectra. In the TA-model we used for absorption phabs model in XSPEC, while in PC-model we used pcfabs in XSPEC for partial covering absorption. The spectral fits were done in XSPEC by tcl scripts.

For each of the above models (*i.e.* NA, TA, and PC models, each with N parameters) we fitted all the spectra with all N parameters free. Example fits to four observed spectra are shown in **Figure 5**. Then the fits were redone by fixing one

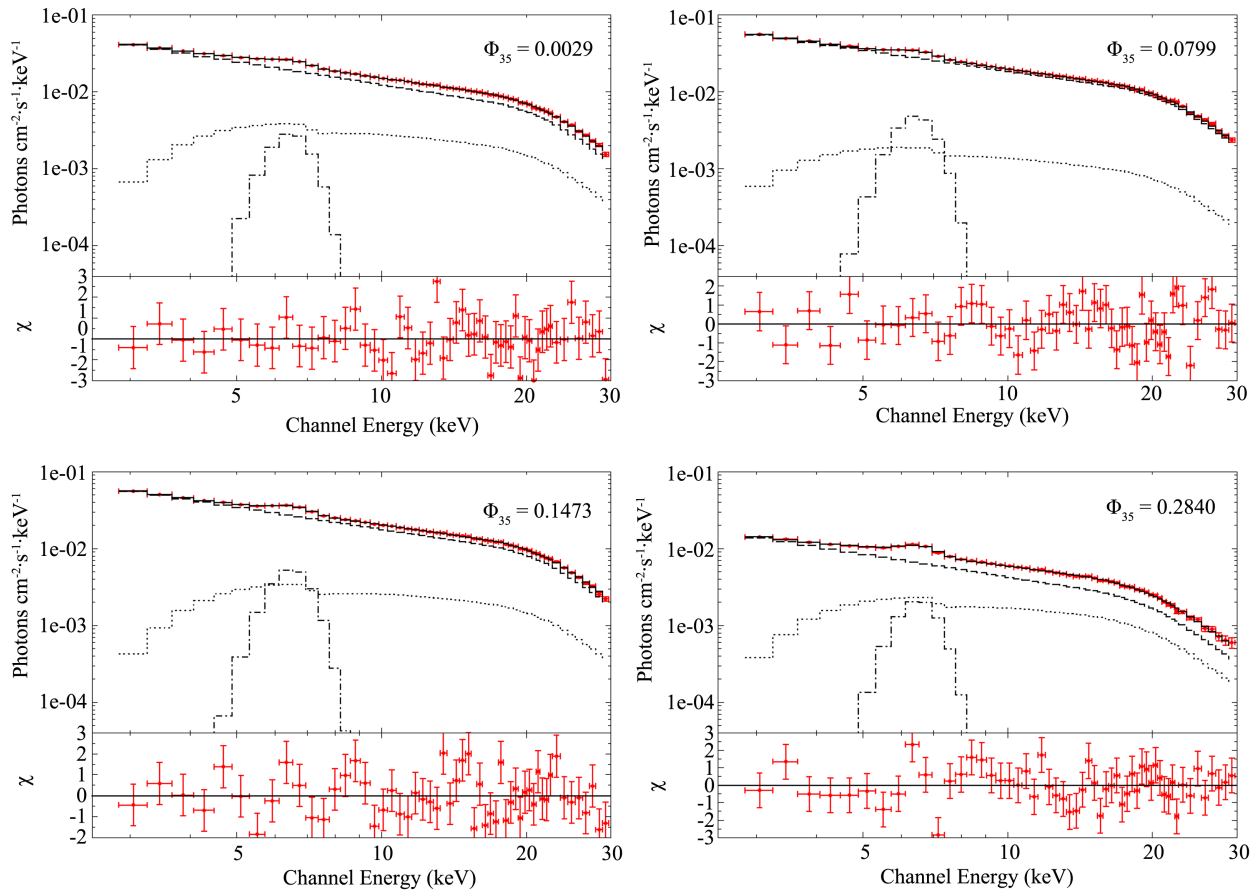


Figure 5. RXTE/PCA spectra and model fits for different 35-day phases (labelled in the upper-right corner of each panel). The spectral model is the PC model with all spectral parameters free.

parameter. This was done for each of the spectral parameters. We compared the χ^2 for fits with a particular parameter fixed compared χ^2 for fits with that same parameter free. The parameter with the lowest increase in χ^2 is the one that shows least variation in the spectra, and was then chosen to be fixed. The procedure was repeated with the remaining $N - 1$ spectral parameters to find the second parameter that caused least increase in χ^2 . Then it was repeated for the remaining $N-2$ spectral parameters, and repeated until there were no free parameters.

This procedure resulted in fixing the parameters in the following order of causing lowest increase in χ^2 to higher (but still small) increases in χ^2 : 1) constant Iron line width (labelled W); 2) constant Iron line width and folding energy (labelled WF); 3) constant line width, folding energy and iron line energy (WFL); and 4) constant width, folding, line, and cutoff energies (WFLC). Fixing further parameters beyond four resulted in large increases in χ^2 , thus showing real variations between spectra. Thus, it is not reasonable to fix the remaining parameters and they were left free. The same test procedure was applied to NA, TA and PC models and resulted in the same ordering of parameters that could be fixed.

Next we compared the χ^2 values between the three (NA, TA and PC) models with the aim of determining which is most reasonable to use to represent the spectra of Her X-1. **Figure 6** shows the difference between χ^2 values of NA-model and PC-model fits (χ^2 (NA model) – χ^2 (PC model)) as a function of 35-day phase during Main High state (35-day phase 0 to 0.27).

The NA-model has two more degrees of freedom than PC-model, thus data points in these plots above the threshold of 4.61 for the increase in χ^2 (red line in **Figure 6**) show worse fits, at more than 90% significance, with the NA-model compared to the PC model. In the spectral fits starting from the models with all parameters free to the one with the largest number of fixed parameters (*i.e.* free, W, WF, WFL, and WFLC fits), the percentage of spectra that show better fits with a significance level of 90% for PC-model over the NA-model are 70%, 68%, 74%, 75%, and 88% of the spectra respectively.

A similar comparison was made between the TA-model and PC-model. The difference between χ^2 values of TA-model and PC-model have the same shape as for NA-model compared to PC-model shown in **Figure 6**, except that the χ^2 differences are typically half of the amount found for the NA-model compared to PC-model fits. There is 1-extra degree of freedom in TA-model than in the PC-model, thus the 90% significance level threshold value for the difference in χ^2 is 2.71. Starting from models with all parameters free to the model with largest number of fixed parameters (WFLC), the percentage of data points with difference in χ^2 larger than 2.71 are 53%, 40%, 45%, 49%, and 70% respectively.

We have also tried to fit the spectra with a partial covering absorption by partially-ionized material (zxipcf in XSPEC). The spectral fits using partial covering with a partially-ionized absorber is referred to as IPC-model (Ionized Partial Covering). The partial covering with cold absorber (PC-model) shows better fits

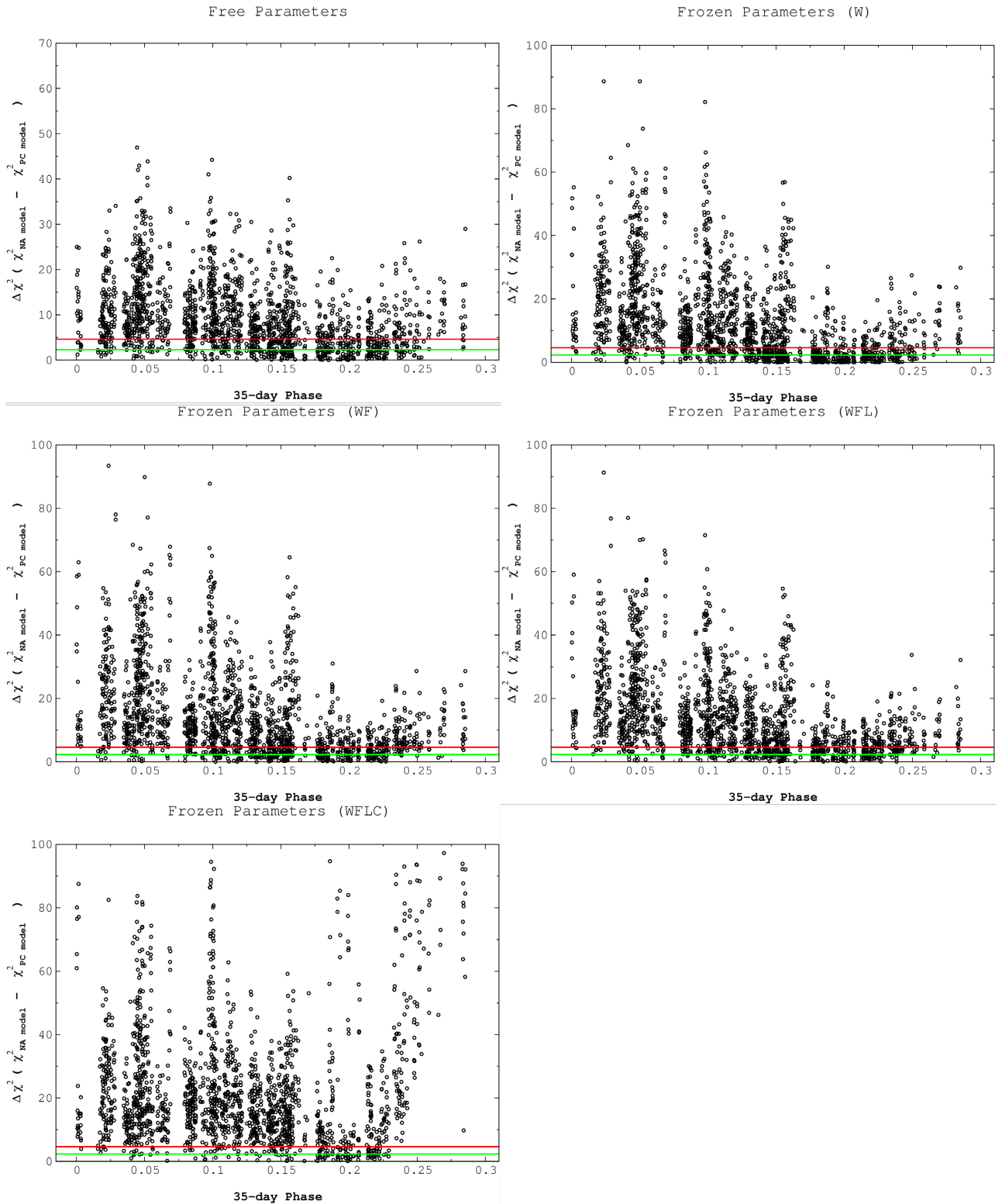


Figure 6. Differences in χ^2 for fits to XTE/PCA spectra with NA model compared to fits with PC model. Each panel shows the difference as a function of 35-day phase, with the fixed parameters (0 to 4 in number) given in the label above each panel.

than IPC-model with 90% significance level in 69% of the spectra and are uniformly distributed over the 35-day phase.

From the above test fits we find that the spectra of Her X-1 in the 2.5 - 30 keV energy range are best described by a two-component power-law with high energy cutoff continuum (unabsorbed and absorbed by a cold absorber) model. This is consistent with previous results, where the two component (absorbed and unabsorbed) was found to be needed throughout the 35-day cycle [23] [24] [25]. Thus we proceeded for the final spectral analysis using the PC-model.

3. Results of Spectrum Modelling

From these test fits the final model chosen is the PC model. We extracted energy spectra from standard-2 data of RXTE/PCA in 129 channels with larger exposure times to 1) reduce the number of spectra and 2) obtain better statistics for each spectrum. To obtain nearly constant signal-to-noise ratios for all spectra, we split the data into time intervals between 400-s and 1360-s with a mean value of 889-s. This resulted in a total of 609-spectra covering 20 MH-state. The extracted spectra include events detected in all layers and columns of the active PCUs combined together. Similarly, all layers and columns of the active PCUs are combined for background files using the faint background model. The corresponding response matrices were created accordingly.

We fit the spectra in the energy range 2.5 - 30 keV with the PC-model consisting of an unabsorbed continuum component and an absorbed component. Both continuum components have the same spectral parameters except for their normalizations. A multiplicative Gaussian line in absorption (*gabs* in XSPEC), was added to the model to smooth the continuum at the cutoff-energy. The energy of the *gabs* function was tied to the cutoff energy, while its width and depth were fixed at 1.5 keV and 0.35 respectively. Another Gaussian line (*gauss* in XSPEC) in emission for the Fe K_{α} line was added to the continuum model. Test fits showed that allowing a free iron line width and folding energy did not improve the fits, thus we fixed the line width and folding energy to 0.6 and 7.8 respectively.

The value of folding energy obtained here is lower than that obtained by [22] of $10.8^{+0.2}_{-0.3}$ and the value obtained by [26] of $10.22^{+/-} 0.07$. Reference [22] studied the spectra of Her X-1 during the peak of the MH-state in 5 hours of observations on MJD 50,705, 35-day phase 0.02 (cycle number 18 in our data) and used data from PCA and HEXTE instruments (with energy ranges 3.5 - 60 keV and 20 - 70 keV, respectively). Reference [26] analyzed data from PCA and HEXTE covering the MH-state (MJD 52,595 to 52,604, 35-day phase 0.01 to 0.25 (cycle number 73 in our data).

There could be a number of reasons responsible for this difference in the folding energy: 1) references [26] and [22] used data from two instruments (PCA/HEXTE) over a larger energy range than was used in our analysis; 2) references [26] and [22] used only data collected by the top layer of the PCA instrument, while we added all three layer of active PCUs; or 3) reference [22] did not use any absorption, while [26] used a total absorption model. We used the same continuum model as theirs but with a partial covering for the absorption.

By revisiting our test fits with different representations for absorption (NA, TA, and PC models) we rule out that the difference in folding energy to be due to different representation for the low energy absorption. In our test fits we found that the mean values obtained for folding energies are 8.59, 8.36, and 8.11 keV for NA, TA, and PC models respectively. Using data either from the top layer of the PCA units or all layers should not result in such a large change in folding energy. Thus the most probable reason for such difference is the different energy ranges used in fitting the spectra.

The folding energy describes the fastness of the exponential decay beyond the cutoff energy. Thus the large decrease in count rates beyond 30 keV (the upper energy limit in our fits) could be responsible for the increase in the value of folding energy in previous work. This does not necessarily mean that their values of folding energy are more correct because there could be an offset in the calibrations for the PCA and HEXTE.

There are seven free spectral parameters in our fits: the partial covering column density and covering fraction, photon-index, continuum normalization, cutoff energy, iron line energy and line normalizations. The time dependence of spectral parameters over the 35-day cycle during MH-state is shown in **Figures 7-13**. In these plots we separated the data by cycle number. The 35-day cycles are numbered after [15].

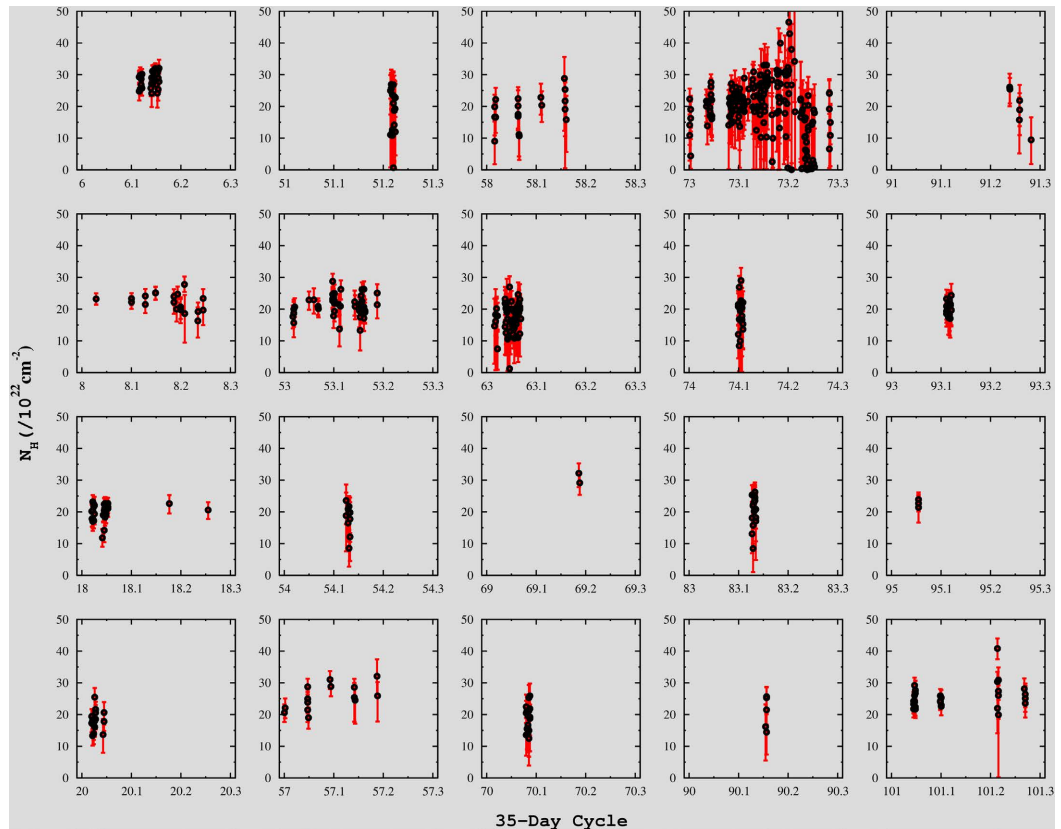


Figure 7. Each panel shows the column density from fits with the partial-covering (PC) model as a function of 35-day phase for the different 35-day main high states.

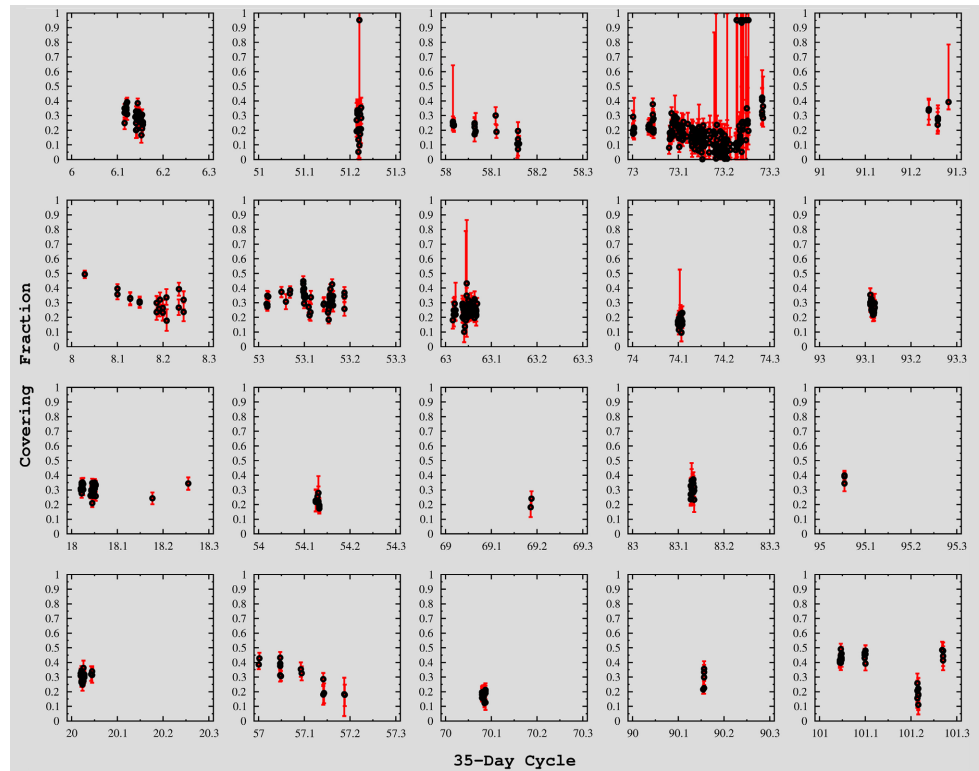


Figure 8. Each panel shows the covering fraction from fits with the PC model as a function of 35-day phase for the different 35-day main high states.

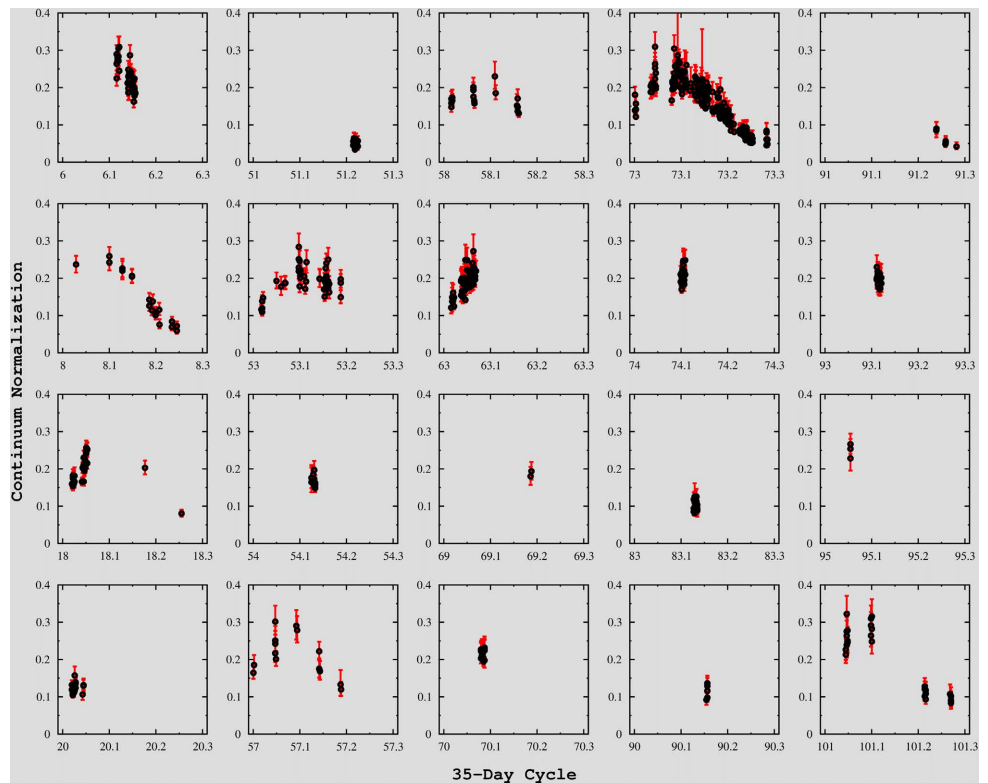


Figure 9. Each panel shows the continuum normalization from fits with the PC model as a function of 35-day phase for the different 35-day main high states.

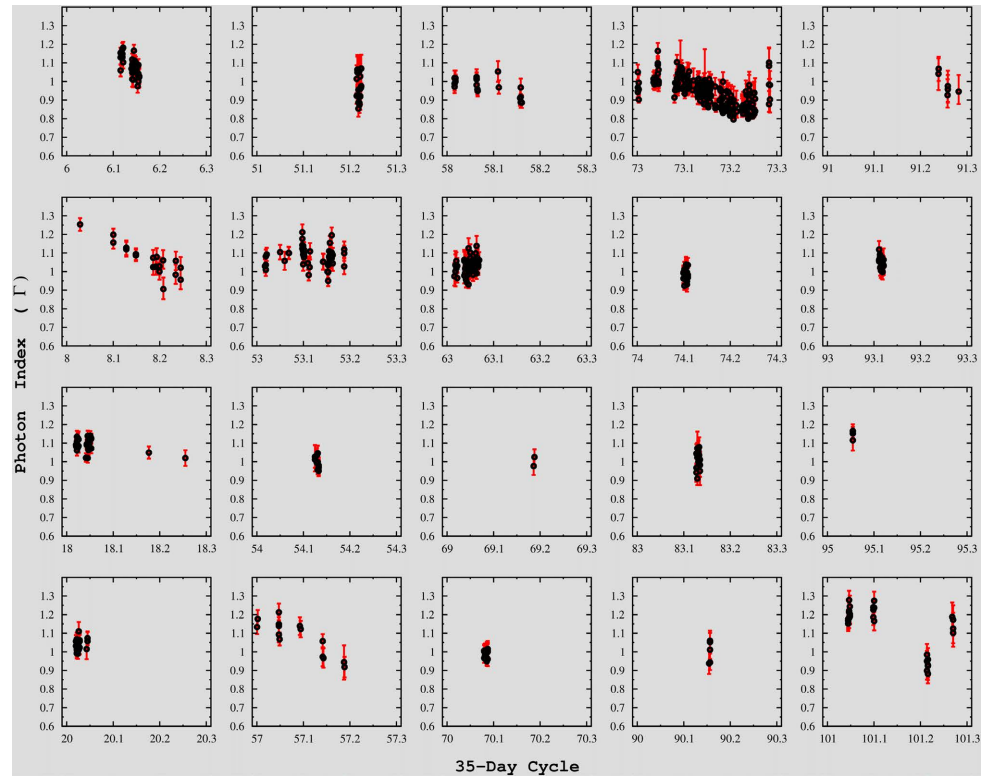


Figure 10. Each panel shows the photon index from fits with the PC model as a function of 35-day phase for the different 35-day main high states.

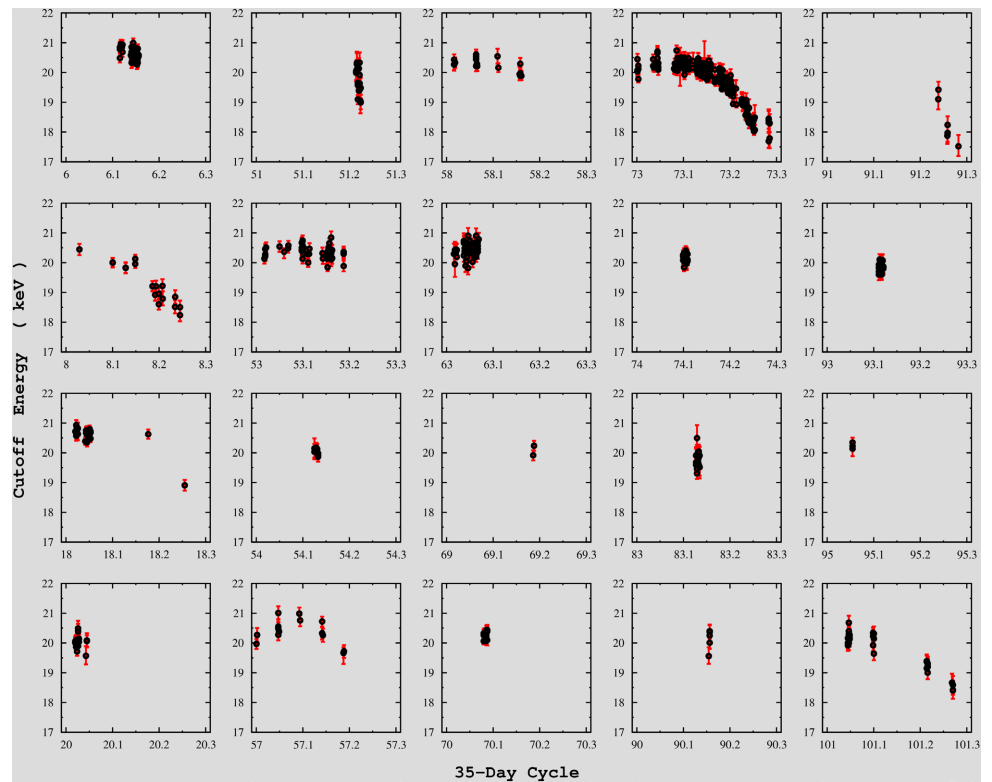


Figure 11. Each panel shows the cutoff energy from fits with the PC model as a function of 35-day phase for the different 35-day main high states.

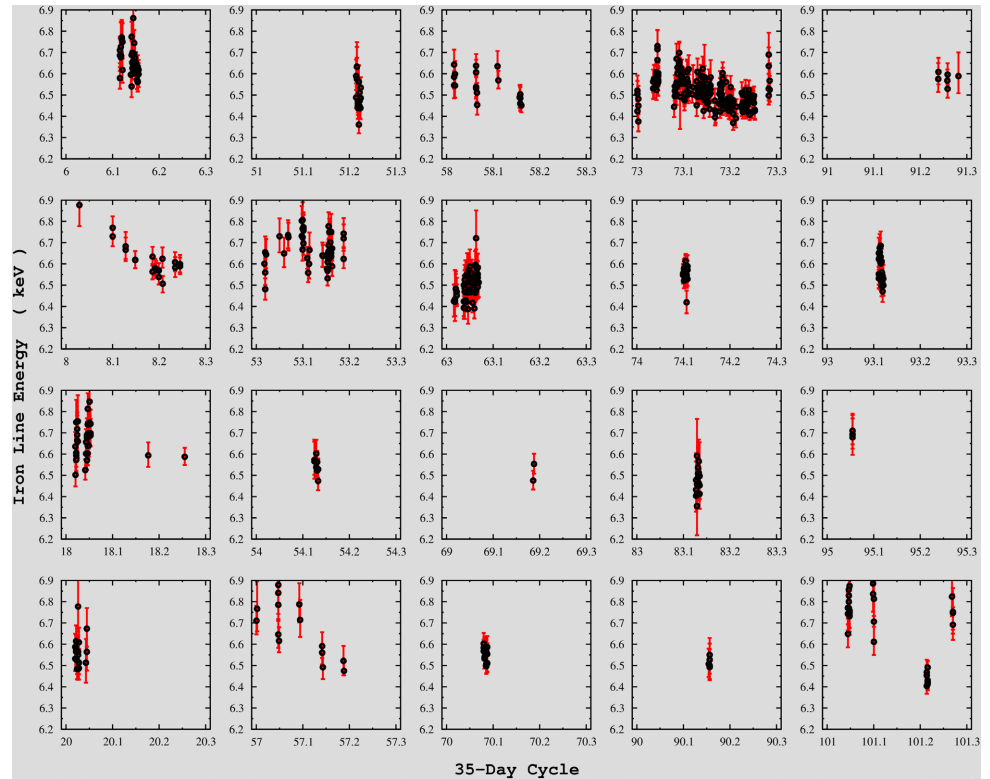


Figure 12. Each panel shows the iron line energy from fits with the PC model as a function of 35-day phase for the different 35-day Main High states.

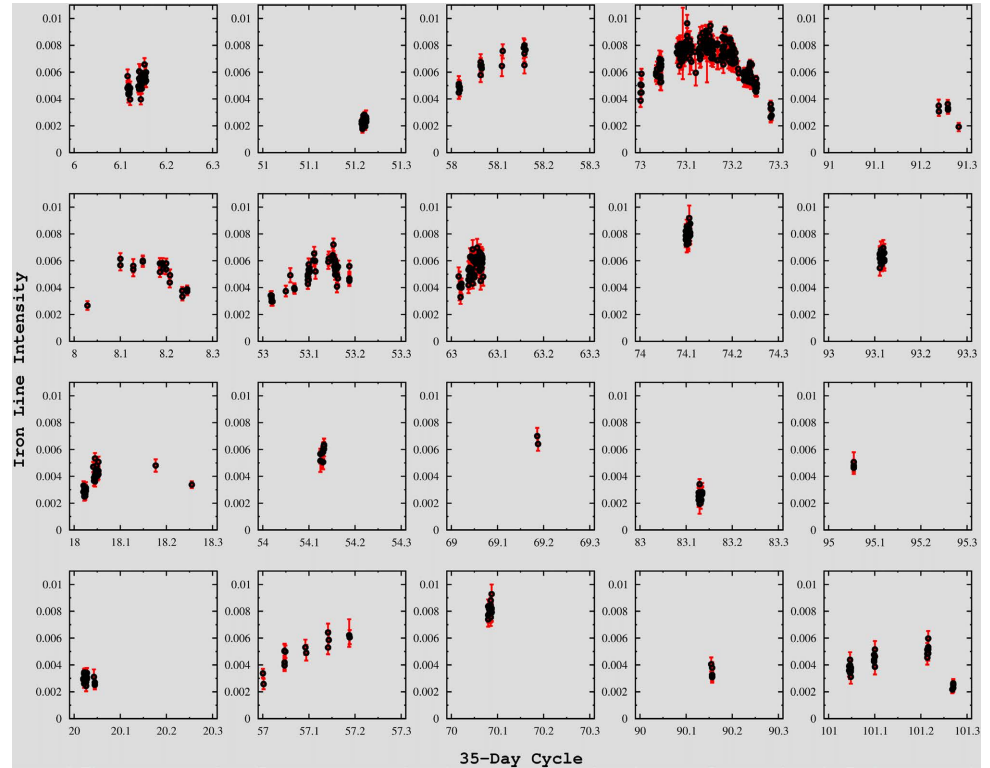


Figure 13. Each panel shows the iron line intensity from fits with the PC model as a function of 35-day phase for the different 35-day Main High states.

Several spectral parameters show a clear evolution with 35-day phase. Because cycle 73 has the most complete coverage of 35-day phase, we compare the other cycles to cycle 73 to estimate whether there is a consistent evolution of a given parameter with 35-day phase during MH state.

The column density (**Figure 7**) has large uncertainties but does not show consistent changes with 35-day phase. For cycle 73 it has values mostly near $2 \times 10^{23} \text{ cm}^{-2}$, but ranges between $1 \times 10^{23} \text{ cm}^{-2}$ and $4 \times 10^{23} \text{ cm}^{-2}$. Other cycles can have similarly high or low values, but the 35-day phase of occurrence of high or low values is different between different cycles. Because column density is known to be related to dips ([16]) and dips occur at different 35-day phases, this is not surprising.

The covering fraction is shown in **Figure 8**. A decrease with 35-day phase from phase 0 to 0.22 is apparent in cycle 73. This is also seen for cycles 8, 57, 58 and 108, with other cycles having too sparse coverage. After 35-day phase 0.22, the covering fraction increases again. A few values of covering fraction values are near 1 with large uncertainties (seen for cycles 51 and 73).

The continuum normalization is shown in **Figure 9**. The continuum normalization would measure the change in strength of the unabsorbed (before absorption) source flux if the other continuum parameters were constant (power-law index and cutoff energy). These other parameters are variable but by small amounts so the continuum normalization is a good proxy for source flux. The shape of the MH state continuum vs. 35-day phase from cycle 73 is well matched by the other cycles, with the rise to peak at 35-day phase 0.1 and subsequent decrease.

The photon index is shown in **Figure 10**. For cycle 73, photon-index has a clear decrease between 35-day phase 0.05 to 0.22. For 35-day phase 0 to 0.05 and 0.22 to 0.3 there are fewer data. The other cycles have some data for these phases, but a clear trend other than the decrease from 0.05 to 0.22 is not seen.

Figure 11 shows the cutoff energy vs. 35-day phase. In most cycles the cutoff energy starts in the early MH-state at high values of 20 - 21 keV and almost stays stable until 35-day phase 0.15, after which it starts to decrease down to 18 keV by the end of MH-state.

Figure 12 shows the iron (Fe K_α) line energy for the different MH states. The iron line originates in gas illuminated by continuum photons with energies high enough to excite the inner shell electrons of iron. Its energy depends on the ionization state of the gas [27]. From cycle 73, there is a clear trend in decrease of iron line energy from 35-day phase 0.05 to 0.22, which indicates a decrease in ionization state of the fluorescing gas. The other cycles show consistency with the behavior of cycle 73.

Figure 13 shows the Fe K_α line intensity. The general trend from cycle 73 is steady increase between 35-day phase 0 to 0.15 followed by a decrease from 35-day phase 0.15 to 0.3. The other cycles are consistent with this trend. There is a clear delay in the increase of line intensity compared to the continuum norma-

lization (shown in **Figure 9**). This is a feature that should be explained by any model for the 35-day cycle. Qualitatively it is telling us that the illumination of the fluorescing gas is different than the illumination by the source in the direction of the observer, thus is providing a constraint on the source, fluorescing gas and observer geometry.

4. Discussion

Based on the disc model by [8] and the pulse evolution model of [3], we can understand the spectra of Her X-1 during the MH-state as being superposition of three components: 1) the spectrum of the direct emission from the pulsar (fan and pencil beams); 2) the spectrum of the reflected X-ray radiation off of the irradiated inner disc ring; and 3) the spectrum of magnetospheric/coronal emission of the scattered direct radiation.

The variation of the relative importance of these components is responsible for the variation of the spectral parameters over the 35-day cycle. Scattered emission, by hot material either in the magnetosphere high above the accretion column or in the corona above and below the accretion disc, is very weak and its energy spectrum is similar to the direct emission. Thus this emission does not contribute significantly to spectral changes during MH-state and SH-state, and is only significant during the low-states.

On the other hand, as can be seen from [8], the reflected emission from the inner disc ring contributes a significant fraction of the observed emission during both high states. The inner disc ring is blocked by the thick-hot atmosphere of the outer disc edge during the early MH-state. The uncovering of the inner ring by this hot-atmosphere is apparent in the gradual increase of its intensity up to 35-day phase 0.15. By the end of MH-state the near side of the inner-disc edge gradually covers the central source and the inner disc ring. Variation of spectral parameters over the 35-day cycle during the MH-state can be explained naturally in this picture.

There are cycles that show deviation from the typical trend of the spectral parameters with 35-day phase (cycle numbers 53, and possibly 51, 90, and 91). These cycles occur after an emergence of the system Her X-1 from an extended low state (*i.e.* Anomalous Low State “ALS”). There are two ALS that occurred in the middle of our observations, during the periods MJD 51255.9 to 51756.9 and 52945.5 to 53159.4 (or in cycle numbers 34 to 48 and 83 to 88). It is generally believed that the ALS results from changes in the state of the accretion disc [28]. Thus the most probable reason for such deviation from the typical trend of spectral evolution is the change in the geometry of the inner disc edge due to proximity of these cycles from ALS periods.

4.1. Cutoff Energy

In the 35-day pulse-evolution model of [3], the reversed fan beam originates at a height of 2 neutron star radii above the neutron star surface and is much broader

in solid angle than the pencil beam (by a factor of about 5 - 10). Both the scattered and reflected emission is dominated by the spectrum of the fan beam. The inner disc ring will be illuminated largely by the fan-beam, so that the backscattered radiation will mostly be that of the incident fan-emission on the inner disc-ring.

Reference [26] carried out a pulse-phase-resolved spectral analysis at 4-intervals over the MH-state (35-day phases 0.03, 0.10, 0.15, 0.20). The cutoff energy variation with pulse phase is shown in **Figure 10** of [26]. The cutoff energy shows a large variation with pulse phase, reaching a high value around the central hard peak (pencil beam) of E_{cut} of 24 - 25 keV and a lower value of E_{cut} of 18 - 22 keV around the leading/trailing shoulders (fan beam).

By considering the phase-resolved variation of the cutoff energy, we expect for early MH-state, when the direct emission is the dominant component, the phase-average spectra will show a high value of the cutoff energy. As the 35-day cycle progresses, the reflected and scattered emission (mostly reflected, and scattered emission of the fan beams) becomes more important and results in a decrease in the pulse-phase-average cutoff energy. This is seen in our results in **Figure 11**.

4.2. Photon Index

For an irradiated slab of cold gas, the incident photons are Compton scattered by free or bound electrons, photoelectrically absorbed and reprocessed into fluorescent line emission and/or destroyed by Auger de-excitation. Because of the decrease of the photo-absorption cross-section with the third power of photon energy, most of the incident soft X-rays are absorbed and a fraction is reprocessed into the fluorescent emission line. On the other hand, higher energy photons are mostly backscattered. Thus, reflected/backscattered radiation by material illuminated by a central X-ray source shows an excess of the continuum above 10 keV [29] [30]. This is a result of electron scattered X-rays, called “the Compton reflection continuum”. One of the main features of the reflected spectrum is the flattening of the spectrum above 10 keV. Figure 1 from [29] shows an example of an incident power law and reflected energy spectra.

As mentioned previously, the evolution of the spectral photon index (**Figure 10**) with 35-day phase generally shows a decreasing trend. The photon index shows higher values (>1.0 , softer spectrum) for the early MH-state up to 35-day phase 0.15. After this phase it shows a decreasing trend (spectra become flatter/harder). This decreasing trend of index is consistent with the increasing fraction of the reflected emission by the inner disc ring as compared to the direct emission from the central source. Although, the energy spectrum of scattered magnetospheric/coronal radiation is similar to the direct radiation, its contribution during MH-state is negligible. This component is responsible for the increase in photon index near the very late end of MH-state (e.g. cycles 73 and 101 in **Figure 10**).

4.3. Iron Line and Continuum Flux

In accreting X-ray pulsars (AXP), the Fe K_{α} line emission is produced by the fluorescent reprocessing of the direct emission from the central source by the surrounding matter. This is indicated by the proportionality between the continuum flux above 7.1 keV and iron line flux [31]. Iron line emission produced by an illuminated slab in reflection is emitted by more highly ionized material near the illuminated face, and thus shows a higher energy fluorescent line. Lines produced in transmission through illuminated material are more likely to be produced far from the illuminated face (*i.e.* in cold material), and thus produce fluorescent lines of lower energy [32].

The possible origins of the Fe K_{α} emission line in Her X-1 during MH-state are: 1) reprocessing of the direct emission in the hot magnetospheric/coronal gas; 2) reprocessing of the direct emission in reflection by the far illuminated face of the inner disc ring; and 3) reprocessing of direct emission and/or reflected emission by the illuminated near side of the inner ring in transmission.

During the decay of the MH-state the near side of the inner disc edge gradually occults the central source first and then the illuminated far side of inner ring. Thus production of the fluorescent iron line in transmission occurs during the decay of MH-state. On the other hand, during the early MH-state the only source for the iron line is the hot material (*i.e.* far side of the inner disc ring illuminated face and/or magnetospheric/coronal gas). This indicates that the Fe K_{α} emission line is expected to have a high energy during the early MH-state and lower energy as 35-day phase increases as found in our observations. The increase in the line energy for the very late MH-state (35-day phase > 0.25) results from the decay of iron line production in reflection/ transmission due to absorption by the near side of the inner disc edge, which completely occults both regions for this phase. Reprocessing in the hot magnetospheric/coronal gas is still present even beyond 35-day phase 0.25. Thus the observed Fe K_{α} line energy change in the RXTE/PCA data results from a varying mixture of two unresolved lines of different energies.

The power-law continuum normalization (Figure 9), shows a faster drop than the iron line intensity (Figure 13) in late MH-state. However, due to the variation of other spectral parameters (including photon index), continuum normalization is not an accurate measure of the continuum strength. We used the “flux” command in XSPEC to calculate the absorption-corrected fluxes of the model within a given energy range from the best-fit spectral parameters and their uncertainties. Figure 14 shows the ratio of 20 - 30 keV continuum flux to the Fe K_{α} line intensity phase for the different MH states. This ratio shows a decrease near the end of MH-state. This decrease can be understood if the occultation of the direct-emission/central-source occurs earlier in the MH state than the occultation of line production regions.

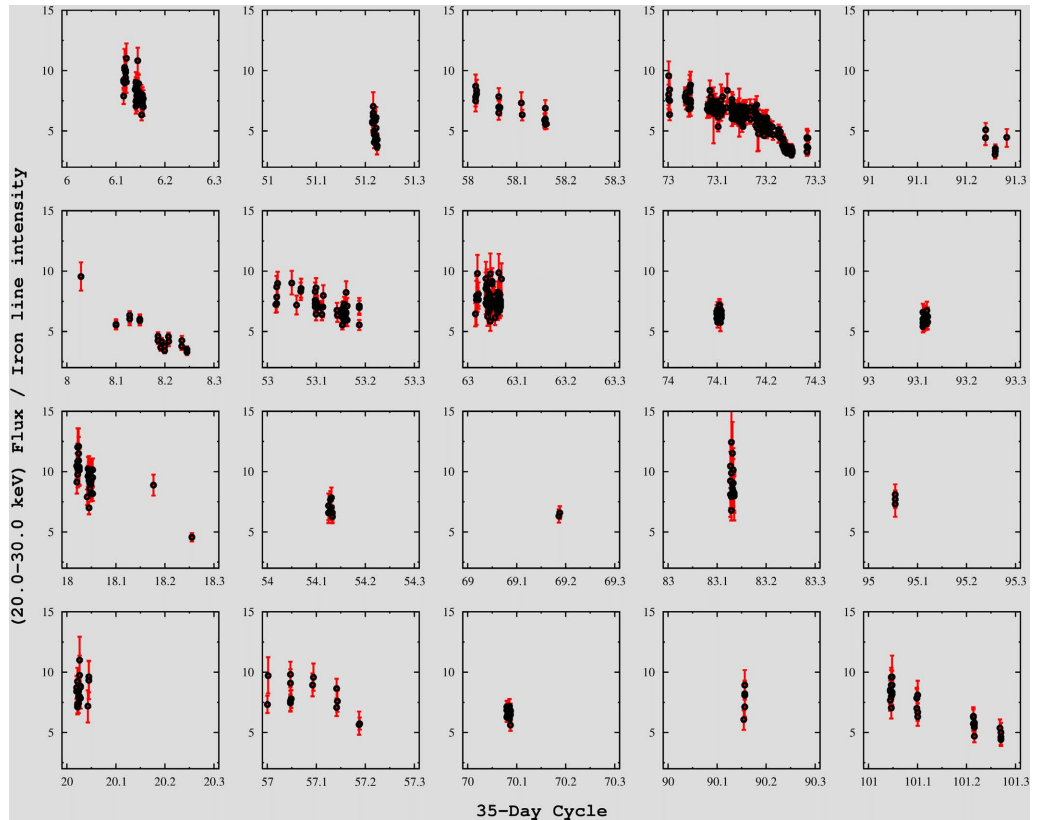


Figure 14. Each panel shows the ratio of 20 - 30 keV continuum flux to iron line intensity as a function of 35-day phase for the different 35-day Main High states.

5. Summary and Conclusions

Her X-1/HZ Her was observed by the RXTE/PCA instrument for 20 different Main High (MH) states over the 19-year period 1996 to 2005. We have obtained the set of observations from the RXTE archive at HEASARC and analyzed the light-curves and spectra of Her X-1 with the goal of characterizing the Main High state of the 35-day cycle.

The low energy (2 - 4 keV) and high energy (9 - 20 keV) light-curves (**Figure 2** and **Figure 3**) show that: one cycle (number 73) has extensive coverage of 35-day phase of MH (35-day phase 0 to ~ 0.3); the other 19 cycles have low coverage; the light-curves are consistent with having nearly the same shape but with different peak intensity (see **Figure 1** for all MH data overlaid); the softness ratio (**Figure 4**) has a consistent shape for all cycles. There are sharp drops in softness ratio which indicate absorption dips [16]: these are not the subject of the current study, so were removed prior to light-curve or spectrum analysis.

To find a universal spectral model which is adequate to describe all MH spectra and allow comparison of spectral parameters with 35-day phase in MH, we carried out a large set of test fits. The model which we find is best to describe MH spectra is the power-law with an exponential cutoff. A fluorescent iron emission line is also required. Partial covering absorption gives a better description than uniform absorption (or no absorption) and we find a neutral absorber

fits the spectra better than an ionized absorber. With this universal spectral model, all MH spectra for the 20 different MH states were fit using χ^2 minimization and the XSPEC software.

The resulting spectral parameters variation with 35-day phase was obtained for MH (**Figures 7-13**). Cycle 73 serves as a prototype for the 35-phase dependence of spectral parameters, but the other 19 cycles are generally consistent with cycle 73. Column density does not show a clear trend with 35-day phase. However, covering fraction has a minimum in late MH at 35-day phase 0.22. Continuum normalization peaks at 35-day phase 0.1, which is peak of MH state. Photon index declines from 1.1 at 35-day phase 0.05 to 0.85 at 35-day phase 0.22, with values near 1.0 for earlier than 0.05 or later than 0.22. Cutoff energy is constant at 20.5 keV for early MH (35-day phase 0 to 0.1) then declines to 18 keV at end of MH. The iron line energy has large errors, but shows a decrease, indicating a less-ionized fluorescing gas, from 35-day phase 0.05 to 0.22. Lastly, we calculated unabsorbed source fluxes for each spectrum and showed the ratio of 20 - 30 keV source flux to iron line intensity in **Figure 14**. This shows a smooth trend of decreasing flux to iron line ratio, indicating more efficient iron line production as 35-day phase increases.

The above trends can be qualitatively described by the precessing-disc occultation model for the 35-day cycle in Her X-1 ([3] [7] [8] [9] [28]) with the most detailed model to date presented by [33]. One goal of the current work is to provide light-curves and spectral parameters vs. 35-day phase for the MH state, which can be compared quantitatively to models for the 35-day cycle.

Acknowledgements

Denis A. Leahy thanks the Natural Sciences and Engineering Research Council of Canada for support.

Conflicts of Interest

The authors declare no conflicts of interest regarding the publication of this paper.

References

- [1] Wang, Y. and Leahy, D. (2022) The Evolution of the Orbital Lightcurve of Hercules X-1 with 35 Day Phase. *The Astrophysical Journal*, **927**, Article No. 143. <https://doi.org/10.3847/1538-4357/ac496f>
- [2] Leahy, D. and Wang, Y. (2021) The 35-Day Cycle of Hercules X-1 in Multiple Energy Bands from MAXI and Swift/BAT Monitoring. *Universe*, **7**, 60. <https://doi.org/10.3390/universe7060160>
- [3] Scott, D., *et al.* (2000) The 35 Day Evolution of the Hercules X-1 Pulse Profile: Evidence for a Resolved Inner Disk Occultation of the Neutron Star. *The Astrophysical Journal*, **539**, 392-412. <https://doi.org/10.1086/309203>
- [4] Scott, D.M. and Leahy, D.A. (1999) Rossi X-Ray Timing Explorer All-Sky Monitor Observations of the 35 Day Cycle of Hercules X-1. *The Astrophysical Journal*, **510**,

- 974-985. <https://doi.org/10.1086/306631>
- [5] Parmar, A.N., Pietsch, W., McKechnie, S., *et al.* (1995) An Extended X-Ray Low State from Hercules X-1. *Nature*, **313**, 119-121. <https://doi.org/10.1038/313119a0>
- [6] Leahy, D.A. (2004) Mass-Radius from a Pulse Shape Model for Hercules X-1. *The Astrophysical Journal*, **613**, 517-521. <https://doi.org/10.1086/422905>
- [7] McCray, R.A., Shull, J.M., Boynton, P.E., *et al.* (1982) Einstein Observatory Pulse-Phase Spectroscopy of HER X-1. *Astrophysical Journal*, **262**, 301-307. <https://doi.org/10.1086/160421>
- [8] Leahy, D.A. (2002) Modelling RXTE/ASM Observations of the 35-d Cycle in Her X-1. *Monthly Notices of the Royal Astronomical Society*, **334**, 847-854. <https://doi.org/10.1046/j.1365-8711.2002.05547.x>
- [9] Leahy, D.A. and Marshall, H. (1999) Extreme-Ultraviolet Explorer Observations of Hercules X-1 at the End of the Short High State. *The Astrophysical Journal*, **521**, 328-331. <https://doi.org/10.1086/307540>
- [10] Leahy, D.A. (2015) Hercules X-1: Using Eclipse to Measure the X-Ray Corona. *The Astrophysical Journal*, **800**, Article No. 32. <https://doi.org/10.1088/0004-637X/800/1/32>
- [11] Bradt, H.V.D. and McClintock, J.E. (1983) The Optical Counterparts of Compact Discrete Galactic X-Ray Sources. *Annual Review of Astronomy and Astrophysics*, **21**, 13-66. <https://doi.org/10.1146/annurev.aa.21.090183.000305>
- [12] Jahoda, K., Swank, J.H. and Giles, A.B. (1996) In-Orbit Performance and Calibration of the Rossi X-Ray Timing Explorer (RXTE) Proportional Counter Array (PCA). *Proceedings of SPIE*, **2808**, 59-70. <https://doi.org/10.1117/12.256034>
- [13] Jahoda, K., Markwardt, C.B., Radeva, Y., *et al.* (2006) Calibration of the Rossi X-Ray Timing Explorer Proportional Counter Array. *The Astrophysical Journal Supplement Series*, **163**, 401-423. <https://doi.org/10.1086/500659>
- [14] Staubert, R., Klochkov, D. and Wilms, J. (2009) Updating the Orbital Ephemeris of Hercules X-1; Rate of Decay and Eccentricity of the Orbit. *Astronomy and Astrophysics*, **500**, 883-889. <https://doi.org/10.1051/0004-6361/200911690>
- [15] Leahy, D.A. and Igna, C.D. (2010) RXTE-Based 35 Day Cycle Turn-On Times for Hercules X-1. *The Astrophysical Journal*, **713**, 318-324. <https://doi.org/10.1088/0004-637X/713/1/318>
- [16] Igna, C.D. and Leahy, D.A. (2011) Hercules X-1's Light-Curve Dips as Seen by the RXTE/PCA: A Study of the Entire 1996 February-2005 August Light Curve. *Monthly Notices of the Royal Astronomical Society*, **418**, 2283-2291. <https://doi.org/10.1111/j.1365-2966.2011.19550.x>
- [17] Leahy, D.A. and Yoshida, A. (1995) Analysis of an Eclipse INGRESS during a High State of Hercules X-1. *Monthly Notices of the Royal Astronomical Society*, **276**, 607-613. <https://doi.org/10.1093/mnras/276.2.607>
- [18] Leahy, D.A. and Igna, C.D. (2011) The Light Curve of Hercules X-1 as Observed by the Rossi X-Ray Timing Explorer. *The Astrophysical Journal*, **736**, Article No. 74. <https://doi.org/10.1088/0004-637X/736/1/74>
- [19] White, N.E., Swank, J.H. and Holt, S.S. (1983) Accretion Powered X-Ray Pulsars. *Astrophysical Journal*, **270**, 711-734. <https://doi.org/10.1086/161162>
- [20] Tanaka, Y. (1986) Observations of Compact X-Ray Sources. *Proceedings of IAU Colloq 89*, Copenhagen, 11-20 June 1985, 198. https://doi.org/10.1007/3-540-16764-1_12
- [21] Mihara, T. (1995) Observational Study of X-Ray Spectra of Binary Pulsars with

- Ginga. Ph.D. Thesis, Dept. of Physics, Univ. of Tokyo, Tokyo.
- [22] Coburn, W., Heindl, W.A., Rothschild, R.E., *et al.* (2002) Magnetic Fields of Accreting X-Ray Pulsars with the Rossi X-Ray Timing Explorer. *The Astrophysical Journal*, **580**, 394-412. <https://doi.org/10.1086/343033>
 - [23] Leahy, D.A., Yoshida, A. and Matsuoka, M. (1994) Spectral Evolution during Pre-Eclipse Dips in Hercules X-1. *Astrophysical Journal*, **434**, 341. <https://doi.org/10.1086/174732>
 - [24] Mihara, T., Ohashi, T. and Makishima, K. (1991) X-Ray Spectrum of Hercules X-1 in the Low State of the 35-Day Cycle. *Publications of the Astronomical Society of Japan*, **43**, 501-501.
 - [25] Leahy, D.A. (2001) Ginga Observations of Hercules X-1: Spectrum Dependence on 35 Day Phase. *The Astrophysical Journal*, **547**, 449-456. <https://doi.org/10.1086/318368>
 - [26] Vasco, D., Staubert, R. and Klochov, D. (2013) Pulse Phase and Precession Phase Resolved Spectroscopy of Hercules X-1: Studying a Representative Main-On with RXTE. *Astronomy & Astrophysics*, **550**, A111. <https://doi.org/10.1051/0004-6361/201220181>
 - [27] Nagase, F., Hayakawa, S., Sato, N., Masai, K. and Inoue, H. (1986) Circumstellar Matter in the VELA X-1/HD 77581 System. *Publications of the Astronomical Society of Japan*, **38**, 547-569.
 - [28] Leahy, D.A. and Dupuis, J. (2010) Extreme Ultraviolet Explorer Observations of Hercules X-1 over a 35 Day Cycle. *The Astrophysical Journal*, **715**, 897-901. <https://doi.org/10.1088/0004-637X/715/2/897>
 - [29] Reynolds, C.S. (1999) Compton Reflection and Iron Fluorescence in Active Galactic Nuclei and Galactic Black Hole Candidates. *Proceedings of High Energy Processes in Accreting Black Holes*, Graftavallen, 29 June-4 July 1998, 178.
 - [30] Makishima, K., Mihara, T., Nagase, F. and Tanaka, Y. (1999) Cyclotron Resonance Effects in Two Binary X-Ray Pulsars and the Evolution of Neutron Star Magnetic Fields. *The Astrophysical Journal*, **525**, 978-994. <https://doi.org/10.1086/307912>
 - [31] Kallman, T.R. (1991) Iron Lines from X-Ray Binaries. *Proceedings of a Workshop*, Varenna, 9-12 October 1990, 85-97. <https://doi.org/10.1007/BFb0031278>
 - [32] Leahy, D.A. (1999) Monte Carlo Calculations of X-Ray Reflection Spectra from a Cloud. *Journal of the Royal Astronomical Society of Canada*, **93**, 33.
 - [33] Leahy, D.A., Postma, J. and Chen, Y. (2020) AstroSat UVIT Observations of Her X-1. *The Astrophysical Journal*, **889**, Article No. 131. <https://doi.org/10.3847/1538-4357/ab65f9>